Arch. Metall. Mater., Vol. 61 (2016), No 3, p. 1483–1488

DOI: 10.1515/amm-2016-0243

M. MOSIAŁEK*#, A. KĘDRA*, M. KRZAN*, E. BIELAŃSKA*, M. TATKO*,

$Ba_{0.5}Sr_{0.5}Co_{0.8}Fe_{0.2}O_{3-\delta}$–$La_{0.6}Sr_{0.4}Co_{0.8}Fe_{0.2}O_{3-\delta}$ COMPOSITE CATHODE FOR SOLID OXIDE FUEL CELL

Composite cathodes contain $Ba_{0.5}Sr_{0.5}Co_{0.8}Fe_{0.2}O_{3-\delta}$ and $La_{0.6}Sr_{0.4}Co_{0.8}Fe_{0.2}O_{3-\delta}$ were tested in different configuration for achieving cathode of area specific resistance lower than $Ba_{0.5}Sr_{0.5}Co_{0.8}Fe_{0.2}O_{3-\delta}$ and $La_{0.6}Sr_{0.4}Co_{0.8}Fe_{0.2}O_{3-\delta}$ cathodes. Electrodes were screen printed on samaria-doped ceria electrolyte half-discs and tested in the three electrode setup by the electrochemical impedance spectroscopy. Microstructure was observed by scanning electron microscopy. The lowest area specific resistance 0.46 and 2.77 Ω cm^{-2} at 700 °C and 600 °C respectively revealed composite cathode contain $Ba_{0.5}Sr_{0.5}Co_{0.8}Fe_{0.2}O_{3-\delta}$ and $La_{0.6}Sr_{0.4}Co_{0.8}Fe_{0.2}O_{3-\delta}$ in 1:1 weight ratio. The area specific resistance of this cathode is characterized by the lowest activation energy among tested cathodes.

Keywords: barium strontium cobalt ferrite; lanthanum strontium cobalt ferrite, solid oxide fuel cell, oxygen reduction reaction, electrochemical impedance spectroscopy

1. Introduction

Nowadays the research concerning solid oxide cells (SOFCs) is focused on intermediate temperature (IT) range (500–700 °C). The slow cathode reaction in this range is a source of main energy losses. The good cathode material should reveal excellent catalytic activity in the oxygen reduction reaction (ORR), high ionic and electronic conductivity and the thermal expansion coefficient (TEC) similar to the TEC of the electrolyte.

$La_{0.6}Sr_{0.4}Co_{0.8}Fe_{0.2}O_{3-\delta}$ (LSCF) and $Ba_{0.5}Sr_{0.5}Co_{0.8}Fe_{0.2}O_{3-\delta}$ (BSCF) cathode materials are extensively studied due their excellent properties [1–10]. The electronic conductivity of LSCF is very high in comparison to other cathode materials, revealing the maximum value of 215.58 S cm^{-1} at 823 K, whereas BSCF reveals much lower electronic conductivity 14.87 S cm^{-1} at 773 K [1]. The ionic conductivity of LSCF and BSCF are enough high in comparison to doped cerias – typical electrolytes for IT–SOFC. LSCF at 1073 K reveal ionic conductivity at the same level as gadolinia-doped ceria (GDC) [2], whereas ionic conductivity of BSCF is even higher than samaria-doped ceria (SDC) ionic conductivity [8]. BSCF reacts with CO_2 present in air, forming oxides and carbonates [9,10]. The TEC of BSCF is much larger than TEC of LSCF [6,7]. Beside BSCF is in several respects a better cathode material than LSCF. Baumann et al. [3, 4] showed that BSCF among BSCF, LSCF, $La_{0.6}Sr_{0.4}CoO_{3-\delta}$, $Sc_{0.5}Sm_{0.5}CoO_{3-\delta}$ and $La_{0.6}Sr_{0.4}FeO_{3-\delta}$ has the lowest surface exchange resistance, for example electrochemical surface exchange resistance at a BSCF microelectrode was 50 times lower than at a LSCF microelectrode of the same geometry. Liu et al. [5] compared anode-supported SOFCs with a GDC electrolyte. These authors showed that a BSCF cathode exhibits a lower interfacial polarization resistance than LSCF cathode in the range (450–600 °C).

Many other new materials are recently reported and its properties are often compared to LSCF or BSCF. The addition of fifth cation at the stage of the synthesis route is one of popular attempts to improve the performance of the cathode [11–17]. Other popular method is development of the composite cathode by addition of the electrolyte material [18–23], silver [9, 24–37], or a $LaCoO_3$ ceramic electronic conductor [38]. Addition of the electrolyte material lead to improvement of the thermal compatibility with the electrolyte due to TEC decrease and ionic conductivity enhancement although in the case of LSCF and BSCF the ionic conductivity of cathode material is even or higher than electrolyte one. The addition of silver to the cathode material lead to decrease of the polarization resistance and increase of the fuel cell performance of both LSCF [24–32] and BSCF [33–35] cathode materials. The addition $LaCoO_3$ to BSCF although improved the electronic conductivity of the cathode, lead to the decrease in the cell performance [38]. The goal of this work is to prepare composite cathode materials contain BCSF and LSCF and check if these materials reveal lower polarization resistance than pure BSCF or LSCF.

2. Experimental

The SDC electrolyte discs 20 mm of diameter, 1 mm thick were prepared as described in [31]. The BSCF powder was obtained by Pechini method as described in [9]. The LSCF (Sigma-Aldridge), BSCF and LSCF–BSCF (1:1 wt. ratio) pastes were prepared from respective powders and

* J. HABER INSTITUTE OF CATALYSIS AND SURFACE CHEMISTRY PAS, CRACOW, POLAND

Corresponding author: nbmosial@cyfronet.pl

organic vehicle (Fuel Cell Materials Inc.). The electrodes were prepared by screen printing appropriate paste on the surface of electrolyte, then left for 24 h, then sintered at 1100 °C, with the 1° min^{-1} heating and cooling rate. On the whole one side of the electrolyte disk the LSCF counter electrode was prepared, then the disk was cut in half and two identical 5 mm of diameter working and reference electrodes at the other side of the half-disk were prepared (Fig. 1). The following cells were prepared and tested, O_2|LSCF|SDC|LSCF|O_2, O_2|LSCF|SDC|BSCF|O_2, O_2|LSCF|SDC|BSCF–LSCF|O_2, (B–L) (the separator "–"means composite of two phases, whereas "|" separate two phases/layers), O_2|LSCF|SDC|LSCF|BSCF–LSCF|O_2 (L|B–L), O_2|LSCF|SDC|BSCF|BSCF–LSCF|O_2 (B|B–L). The cell was mounted as shown in Fig. 1, the sketch of the electrochemical cell and more details of the cell assembly are described elsewhere [9].

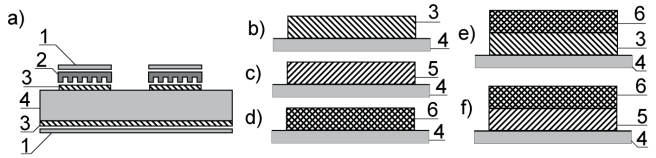

Fig. 1. The schematic view of (a) the cell assembly; (b– f) examined electrodes, 1 – Platinum foil, 2 – SUS 430 stainless steel current collector, 3 – LSCF electrode, 4 – SDC electrolyte, 5 – BSCF electrode, 6 – BSCF–LSCF composite electrode; (b) LSCF electrode; (c) BSCF electrode; (d) BSCF–LSCF composite electrode; (e) LSCF|BSCF–LSCF (L|B–L) electrode, (f) BSCF|BSCF–LSCF (B|B–L) electrode

The electrodes were connected to the Gamry 300 series potentiostat/galvanostat/ZRA. Electrochemical experiments were performed in oxygen (99.5% Linde gaz Polska) or mixtures of oxygen and argon (99.999 Linde gaz Polska) with 150 cm^3 min^{-1} flow rate in the 500–700 °C range. The frequency range used in EIS measurements was from 0.01 to 300 000 Hz at the logarithmic frequency steps of ten points per decade. The amplitude of the sinusoidal voltage signal was 20 mV. In the analysis of the registered impedance data the program Minuit [39] based on a non-linear least-square regression procedure was used. The program Minuit was adjusted to fit an equation describing the assumed equivalent electrical circuit (EEC) to the measured data. The error was characterized by the standard deviation *s*, calculated from the formula:

$$s = \sqrt{\frac{\sum_{1}^{n}\left(\frac{\text{Modulus}(Z_{i,measured} - Z_{i,fitted})}{\text{Modulus}(Z_{i,measured})}\right)^2}{n-1}} \qquad (1)$$

where Z_i means the impedance at the frequency number *i* and *n* is the number of frequencies in the impedance spectrum.

3. Results and discussion

Prepared electrodes contain well connected grains with enough large inter-grain voids to ensure easy access of oxygen to the whole electrode surface (Fig. 2). The LSCF electrodes were more thermal shock resistant than BSCF ones due to lower difference of electrode and electrolyte TECs. The examples of impedance spectra in Nyquist representation of the examined electrodes are presented in Fig. 3.

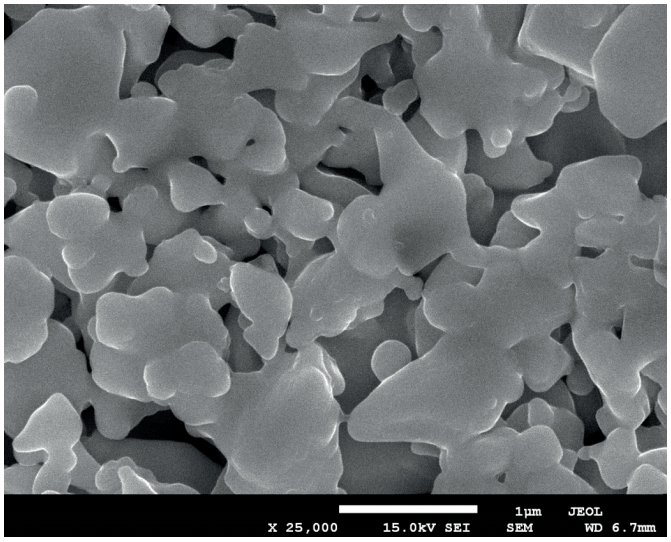

Fig. 2. SEM micrographs of the LSCF electrode

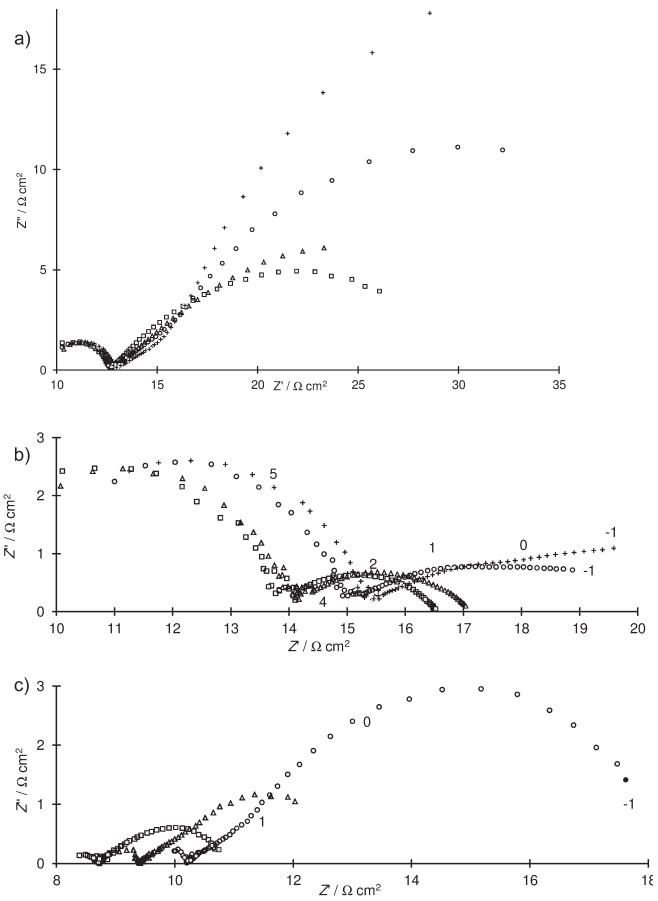

Fig. 3. Examples of EIS spectra in the Nyquist representation at various oxygen concentrations: squares P_{O2}/P =1, triangles P_{O2}/P =0.1, circles P_{O2}/P =0.01 and crosses P_{O2}/P =0.005; (a) for the LSCF electrode at 700 °C; (b) for the BSCF–LSCF electrode at 600 °C; (c) for the LSCF|BSCF–LSCF electrode at 600 °C. The numbers along the spectra denote logarithm of frequency

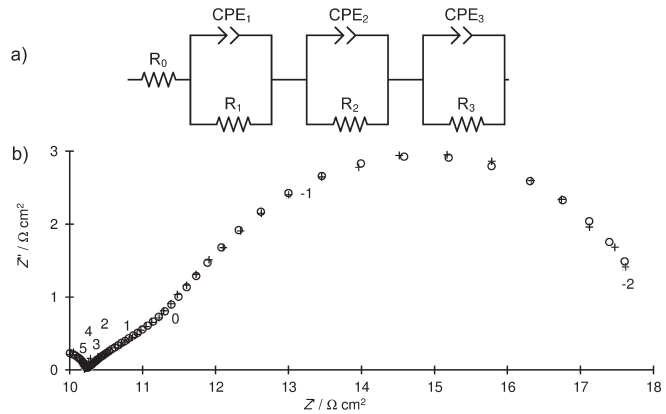

Fig. 4. (a) Equivalent electrical circuit (EEC) used for fitting impedance spectra; (b) example of the fit: LSCF|BSCF–LSCF electrode at 700 °C and $P_{O2}/P = 0.01$; crosses – measured data, circles – fitted data, the numbers near filled symbols denote the logarithm of the frequency

Recorded spectra consist of up to 3 capacitive semicircles. Some of these semicircles are depressed and/or overlapped. Each semicircle can be connected with at least one process/reaction step enough slow to influence the overall reaction speed. The used EEC and an example of a fit are presented in Fig. 4. Each semicircle is represented by a pair of a resistor and a capacitor parallel connected (R_i, C_i). Each capacitor is replaced by a constant phase element (CPE) which impedance may be expressed by the following formula [40]:

$$Z_{CPE_i} = \frac{1}{2\pi f_0 C_i}\left(\frac{f_0}{\mathrm{j}f}\right)^{\alpha} \tag{2}$$

where j is imaginary unit, f is the frequency, f_0 is the frequency of reference, C_i is the capacitance at the frequency of reference, index i is the number of (R, CPE) pair and α is a coefficient close to 1 for an ideal capacitor and usually assuming a value between 0.8–1.0 for the double layer capacitance and close to 0.5 for capacitances connected to diffusion processes. In this work is assumed f_0=1 kHz. The resistor R_0 represents resistance of cable connecting electrodes with potentiostat, current collector and resistance of electrolyte grains. The (R_1, CPE_1) pair connected with high frequency arc is ascribed to the resistance of electrolyte grain boundaries. (R_2, CPE_2) and (R_3, CPE_3) pairs connected with the medium and low frequency arcs respectively are ascribed to electrode processes. The sum of resistances R_2+R_3 gives polarization resistance R_{pol} also called area specific resistance. The calculated polarization resistances examined electrodes are presented in Table 1.

TABLE 1

R_{pol} / Ω cm^{-2} examined electrodes

T / °C	LSCF	BSCF	B–L	L|B–L	B|B–L
700	2.1	14	0.46	2.4	3.6
600	18	76	2.8	–	12

The lowest results are obtained for BSCF–LSCF composite electrode due to high catalytic activity of BSCF particle and excellent electronic conductivity of LSCF particle which ensure current collection from whole cathode. The highest polarization resistances are obtained for BSCF cathode. In this work the SUS 430 stainless steel current collector was used for all examined electrodes. In IT range stainless steel interconnectors could be used, because they are cheaper, provide a higher mechanical stability and are more easily machinable than the ceramic interconnects [41]. The limited contact area between an electrode and a current collector impacts on the cell performance [42]. BSCF electrodes exhibited significant differences in the performance, depending on the type of the current collector used [43]. The LSCF electrodes are much less dependent of the current collector used due to its high electronic conductivity. The obtained R_{pol} LSCF electrodes are similar to reported by Adler et al. [44]. Cathodes with the additional BSCF or LSCF layer between electrolyte and B–L composite are not as good as pure B–L cathodes showed R_{pol} of the same order as pure LSCF cathodes.

The resistance R_i depends on oxygen concentration according to the following formula:

$$\log(R_i) = a - m\log(P_{O2}) \tag{3}$$

where a and m are coefficients. The value of m can be used for the identification of the type of a corresponding process [9, 45–48]. Coefficients m are presented in Table 2.

TABLE 2

Coefficients m calculated for selected resistances

T / °C	LSCF, R_2	LSCF, R_3	LSCF, R_2+R_3	BSCF, R_2+R_3	B–L, R_2+R_3
700	0.03	0.42	0.24	0.20	0.21
600	0.32	0.14	0.15	0.10	0.13

The spectra of the LSCF electrode consist of two well separated semicircles. The medium frequency arc at 700 °C is almost oxygen concentration independent whereas for R_3 m is close to 0.5, it means that this semicircle is related to the diffusion process [44]. Different ORR mechanism is observed at 600 °C at LSCF electrode. Both processes slightly depend on oxygen concentration it cans mean that atomic oxygen is involved in the rate-determining step [48]. MF and LF are strongly overlapped at the impedance spectra of BSCF and B–L electrodes, causing that individual values of R_2 and R_3 carry large experimental errors whereas their sum (R_{pol}) is enough precisely calculated. Coefficients m for R_{pol} of B–L composite electrode are slightly higher than for BSCF one. The temperature dependence of the polarization resistances is plotted in Fig. 5. The activation energies are 64.0, 46.0 and 33.5 kJ mol^{-1} for LSCF, BSCF and B–L electrodes respectively. The activation energy for oxygen diffusion in BSCF is 46.0 kJ mol^{-1} [8], it points that this process is the rate determining step in the ORR at the BSCF cathode.

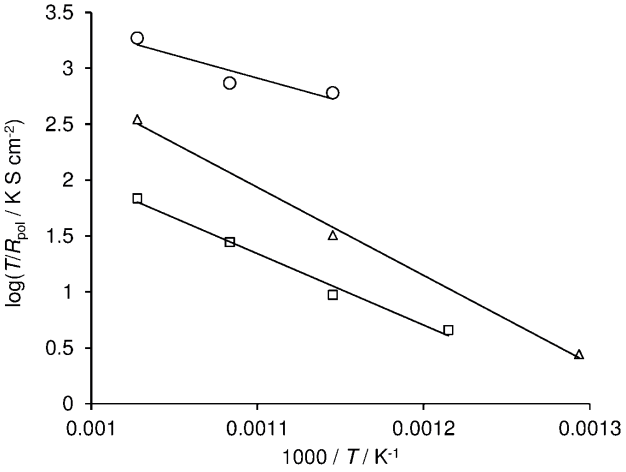

Fig. 5. Arrhenius plot of the electrode reaction resistance (R_2+R_3), squares BSCF electrode, triangles LSCF electrode, circles BSCF–LSCF composite electrode

4. Conclusions

Several composite cathodes contain LSCF and BSCF were tested and compared with BSCF and LSCF cathodes. The lowest polarization resistance exhibited composite cathode obtained by mixing BSCF and LSCF powder in 1:1 weight ratio. This cathode reveals also the lowest activation energy of polarization resistance, so it should also be suitable for use in lower temperatures. The polarization resistance of the composite BSCF–LSCF cathode rises with the decrease of oxygen concentration in a similar manner as R_{pol} of the BSCF cathode.

REFERENCES

[1] A. Jun, S. Yoo, O.-h. Gwon, J. Shin, G. Kim, Electrochim. Acta 89, 372-376 (2013).
[2] S. Wang, M. Katsuki, M. Dokiya, T. Hashimoto, Solid State Ionics 159, 71-78 (2003).
[3] F.S. Baumann, J. Maier, J. Fleig, Solid State Ionics 21-26, 1198-1204 (2008).
[4] F.S. Baumann, J. Fleig, H.-U. Habermeier, J. Maier, Solid State Ionics 177, 3187-3191 (2006).
[5] Q.L. Liu, K.A. Khor, S.H. Chan, J. Power Sources 161, 123-128 (2006).
[6] M. Kuhn, S. Hashimoto, K. Sato, K. Yashiro, J. Mizusaki, Solid State Ionics 241, 12-16 (2013).
[7] W. Zhou, R. Ran, Z. Shao, J. Power Sources 192, 231-246 (2009).
[8] Z. Shao, S.M. Haile, Nature 431, 170-173 (2004).
[9] M. Mosiałek, M. Dudek, A. Michna, M. Tatko, A. Kędra, M. Zimowska, J. Solid State Electrochem. 18, 3011-3021 (2014).
[10] K. Schmale, J. Barthel, M. Bernemann, M. Grünebaum, S. Koops, M. Schmidt, J. Mayer, H.-D. Wiemhöfer, J. Solid State Electrochem. 17, 2897-2907 (2013).
[11] X. Meng, B. Meng, X. Tan, N. Yang, Z.-F. Ma, Mater. Res. Bull. 44, 1293-1297 (2009).
[12] G. Wenyuan, S. Juncai, L. Sha, L. Yang, L. Changmin, T. Nailing, J. Rare Earth. 24, 288-292 (2006).
[13] N. Lakshminarayanan, H. Choi, J.N. Kuhn, U.S. Ozkan, Appl. Catal. B-Environ. 103, 318-325 (2011).
[14] X. Ding, X. Kong, J. Jiang, C. Cui, X. Guo, Mater. Res. Bull. 45, 1271-1277 (2010).
[15] S. Li, Z, Lü, B. Wei, X. Huang, J. Miao, G. Cao, R. Zhu, W. Su, J. Alloys Compd. 426, 408-414 (2006).
[16] S.K. Burnwal, P. Kistaiah, Bonfring International Journal of Industrial Engineering and Management Science 3, 20-23 (2013).
[17] J. Cheng, J. Dong, Q. Jiang, R. Wang, J. Gao, J. Alloys Compd. 521, 45-49 (2012).
[18] B.F. Angoua, E.B. Slamovich, Solid State Ionics 212, 10-17 (2012).
[19] J. Nielsen, T. Jacobsen, M. Wandel, Electrochim. Acta 56, 7963-7974 (2011).
[20] H. Zhao, L. Huo, L. Sun, L. Yu, S. Gao, J. Zhao, Mater. Chem. and Phys. 88, 160-166 (2004).
[21] A. Esquirol, J. Kilner, N. Brandon, Solid State Ionics 175, 63-67 (2004).
[22] H.J. Hwang, J.-W. Moon, S. Lee, E.A. Lee, J. Power Sources 145, 243-248 (2005).
[23] N. Li, A. Verma, P. Singh, J.-H. Kim, Ceram. Int. 39, 529-538 (2013).
[24] S. Wang, T. Kato, S. Nagata, T. Honda, T. Kaneko, N. Iwashita, M. Dokiya, Solid State Ionics 146, 203-210 (2002).
[25] J. Zhang, Y. Ji, H. Gao, T. He, J. Liu, J. Alloys Compd. 395, 322-325 (2005).
[26] Y. Sakito, A. Hirano, N. Imanishi, Y. Takeda, O. Yamamoto, Y. Liu, J. Power Sources 182, 476-481 (2008).
[27] Q. Xu, D.-p. Huang, W. Chen, J.-h. Lee, B.-h. Kim, H. Wang, R.z. Yuan, Ceram. Int. 30, 429-433 (2004).
[28] Y. Liu, S. Hashimoto, K. Yasumoto, K. Takei, M. Mori, Y. Funahashi, Y. Fijishiro, A. Hirano, Y. Takeda, Curr. Appl. Phys. 9, S51-S53 (2009).
[29] S.-H. Jun, Y.R. Uhm, R.-H. Song, C.K. Rhee, Curr. Appl. Phys. 11, S305-S308 (2011).
[30] T.-J. Huang, X.-D. Shen, C.-L. Chou, J. Power Sources 187, 348-355 (2009).
[31] M. Mosiałek, M. Dudek, J. Wojewoda-Budka, Arch. Metall. Mater. 58, 275-281 (2013).
[32] M. Mosiałek, M. Tatko, M. Dudek, E. Bielańska, G. Mordarski, Arch. Metall. Mater. 58, 1341-1345 (2013).
[33] Y. Lin, R. Ran, Z. Shao, Int. J. Hydrogen Energy 35, 8281-8288 (2010).
[34] W. Zhou, R. Ran, Z. Shao, R. Cai, W. Jin, N. Xu, J. Ahn, Electrochim. Acta 53, 4370-4380 (2008).
[35] W. Zhou, R. Ran, R. Cai, Z. Shao, W. Jin, N. Xu, J. Power Sources 186, 244-251 (2009).
[36] M. Dudek, M. Mosiałek, G. Mordarski, R.P. Socha, A. Rapacz-Kmita, Arch. Metall. Mater. 56, 1249-1255 (2011).
[37] M. Mosiałek, M. Przybyła, M. Tatko, P. Nowak, M. Dudek, M. Zimowska, Arch. Metall. Mater. 58, 1337-1340 (2013).
[38] W. Zhou, Z. Shao, R. Ran, P. Zeng, H. Gu, W. Jin, N. Xu, J. Power Sources 168, 330-337 (2007).
[39] F James, M. Roos, Comput. Phys. Commun. 10, 343-367 (1975).
[40] W. Simka, M. Mosialek, G. Nawrat, P. Nowak, J. Żak, J. Szade, A. Winiarski, A. Maciej, L. Szyk-Warszynska, Surf. Coat. Tech. 213, 239-246 (2012).
[41] E. Bucher, C. Gspan, F. Hofer, W. Sitte, Solid State Ionics 230,

7-11 (2013).
[42] S.P Jiang, J.G. Love, L. Apateanu, Solid State Ionics 160, 15-26 (2003).
[43] Y. Guo, Y. Liu, R. Cai, D. Chen, R. Ran, Z. Shao, Int. J. Hydrogen Energy 37, 14492-14500 (2012).
[44] S.B. Adler, J.A. Lane, B.C.H. Steele, J. Electrochem. Soc. 143, 3554-3564 (1996).
[45] M. Tatko, M. Mosiałek, A. Kędra, E. Bielańska, M. Ruggiero-Mikołajczyk, P. Nowak, J. Solid State Electrochem. 20, 143-151 (2016).
[46] B. Philippeau, F. Mauvy, C. Nicollet, S. Fourcade, J.C. Grenier, J. Solid State Electrochem. 19, 871-882 (2015).
[47] X. Xu, C. Cao, C. Xia, D. Peng, Ceram. Int. 35, 2213-2218 (2009).
[48] B. Liu, Y. Zhang, L. Zhang, Int. J. Hydrogen Energy 34, 1008-1014 (2009).